THE JOURNAL OF PHYSICAL CHEMISTRY B

Article

Cite This: J. Phys. Chem. B 2019, 123, 4757−4765

pubs.acs.org/JPCB

Thermotropic Phase Transitions in Butyltrimethylammonium Bis(trifluoromethylsulfonyl)imide Ionic Liquids are Dependent on Heat Flux

Jaclyn N. Curry* and Scott K. Shaw

Department of Chemistry, University of Iowa, Iowa City, Iowa 52245, United States

Supporting Information

ABSTRACT: Transmission infrared spectroscopy (IR) and differential scanning calorimetry are used to identify and characterize multiple phase transitions of butyltrimethylammonium bis(trifluoromethylsulfonyl)imide ([N1114] [TFSI]). Phase-dependent properties are analyzed using temperature-controlled transmission IR, in which we identify changes in the molecular arrangements at and around phase transition temperatures between −80 and 30 °C, which span crystallization and melting phase transitions. Our data report the dependence of phase transition behavior across multiple heat flow rates and the resulting molecular organizations that are formed. This is significant as temperature-specific organizations and properties of ionic liquids (ILs) contribute significantly to their application in separations and in devices. We also identify and discuss the relationship between phase transition temperatures and classes of those transitions when various temperature ramp rates are applied. Our analysis indicates that these relationships of IL thermochemistry could be developed as a diagnostic for assigning phase transition types.

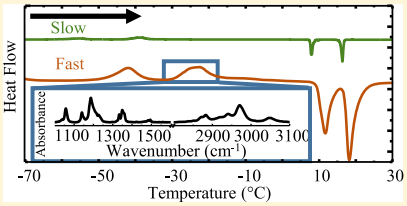

1. INTRODUCTION

Ionic liquids (ILs) are salts with melting points at or near room temperatures. They are generally composed of bulky and asymmetric cations and anions which have several unique physicochemical properties including negligible vapor pressure, high thermal stability, and moderate conductivity.[1−6]

Temperature swings associated with many potential applications[1,4,7−12] can approach or exceed the near-ambient temperatures of many IL phase transitions. Moreover, the heating or cooling rate at which these transitions are met, that is, the heating flux, can lead to variable expression of phases.[13−16] It is important to identify and understand these thermotropic effects so that ILs can be judiciously applied.[17] This research combines calorimetry and vibrational spectroscopy to examine the temperature ramp rate dependence on phase transitions of the IL butyltrimethylammonium bis(trifluoromethylsulfonyl)imide ([N1114] [TFSI]).

Three general classes of ILs have been proposed based on their thermochemistry behaviors.[16] The class is typically determined by examining the thermogram and assigning the phase changes by characteristic traits. Melting phase changes are distinguished by a (negative) endothermic feature while crystallization phase changes are indicated by (positive) exothermic peaks. Glass transitions are observed as a change in a thermogram baseline, which is attributed to a change in the heat capacity between a crystalline or amorphous state.[17,18] ILs are also prone to super cooling.[19] This is evident in cold crystallization (exothermic) features that only present when heating a sample from a supercooled state.[13]

ILs of the first class display relatively simple thermochemistry with clear crystallization points and no glass transitions. The second class of ILs have observable glass transitions, but no distinguishable crystallization or melting phase transitions, indicating that the solid phase remains isotropic. The third class is characterized by the lack of a crystallization phase transition while cooling but upon heating displays one or more of glass transitions and cold crystallizations and finally a melting phase transition. ILs of the third class are interesting because differences in the scanning rate and water content can effect changes in the structure that correlate with phase transitions. Prior research has investigated effect phase transitions on this class of ILs. Infrared (IR) measurements by Hüfft et al. report structures of 1-ethyl-2-methylimidazolium bis(triflouromehtylsulfonyl)imide ([EMIM] [TFSI]) in bulk liquid, thin liquid film, and crystalline solid states.[20] The liquid and crystalline [EMIM] [TFSI] IR spectra show similar spectral features, but the vibrational modes of CF_3 and SO_2 asymmetric stretching vary in intensity and position as a function of physical form. The thin liquid film and crystalline IL exhibit sharper vibrational modes when compared to the bulk liquid, supporting the conclusion that the CF_3 and SO_2 groups are directly involved in the cation−anion interaction in the crystalline state. Specifically, the authors predict that the crystalline state directs the TFSI anion's oxygen atoms to interact with the [EMIM] cation ring structure. The authors conclude that this preferred location of the oxygen with respect to the ring's CH groups could be the driving force behind the crystalline structure.[20]

Research by Ribeiro et al. exploring varying cooling rates on crystallization phase transitions in [N1114] [TFSI] has been

Received: February 20, 2019
Revised: May 7, 2019
Published: May 15, 2019

DOI: 10.1021/acs.jpcb.9b01650
J. Phys. Chem. B 2019, 123, 4757−4765

integral in understanding the third class of ILs.[13] They have analyzed IL phase transitions over "slow" cooling rates of 1 °C min^{-1} and "fast" rates of 5 °C min^{-1}, concluding that faster cooling prohibits complete crystallization.[13] The faster cooling data show a second cold crystallization upon heating.[13] Raman spectroscopy coupled with DFT calculations reveal that cooling at 1 °C min^{-1} resulted in cisoid crystallization of the [TFSI] anion. However, cooling at 5 °C min^{-1} first resulted transoid [TFSI] crystallization, followed by a solid−solid phase transition to the cisoid form as the sample was warmed.[13] An IL used in applications that require temperature change can lead to malfunctions if the structure changes of the IL are not studied and understood.

Based on complex crystallization dependence shown in previous work, our research aims to report the cooling and heating rate dependence on phase transitions for IL [N1114] [TFSI]. We monitor the structural changes during phase transitions using differential scanning calorimetry (DSC) to determine thermal events (crystallization, glass transition, melting, etc.) present when cooling and heating the [N1114] [TFSI] sample at different rates (1 through 15 °C min^{-1}). Temperature-controlled transmission vibrational spectra are also collected to determine the structure of IL at temperatures post thermal events as observed in DSC scans. The collaboration of DSC measurements and temperature-controlled vibrational spectra reveal fundamental differences in phase transitions and possibly a novel technique in understanding how an IL is affected by temperature.

2. EXPERIMENTAL SECTION

The IL butyltrimethylammonium bis(trifluoromethylsulfonyl)-imide, [N1114] [TFSI], is purchased from IoLiTec (USA) at 99% purity. The water content in the IL is 370 ± 160 ppm, which is determined by using three 200 mg aliquots to record KF measurements on a Metrohm 831 Karl Fischer (KF) coulometric titrator. A Hydranal Water Standard 1.0 (Fluka Analytical) is used to calibrate the KF titrator on a regular basis.

The thermal analysis is completed using a TA Instruments (New Castle, DE, USA) Q100 differential scanning calorimeter with liquid nitrogen cooling accessory. Samples are prepared by pipetting ca 4 mg (Sartorius balance 0.1 mg uncertainty) of IL into a preweighed aluminum sample pan which is capped with an aluminum lid and sealed with an encapsulating press. The mass of the empty aluminum pan is subtracted from the sample-filled aluminum pan to determine the sample weight, which is used to determine enthalpy of phase transitions. A clean, empty aluminum pan is used during each measurement as a reference. The sample chamber is purged with a 1:1 mixture of ultrapure helium (Praxair 99.998%) and ultrapure nitrogen (Praxair 99.998%) at 20 mL min^{-1}. Each sample is held for 30 min at 120 °C to drive off water from the pan exterior and the other surfaces. The sample is then cooled to 30 °C at a rate of 10 °C min^{-1} and allowed to equilibrate there. Each measurement consists of cooling the sample to −75 °C and then heating to 30 °C. The cooling rates examined are 5, 10, and 15 °C min^{-1}. Each cooling rate measurement is followed by one of the heating rates, which include 2, 5, 10, and 15 °C min^{-1}. Measurements are replicated at least three times on independent samples to ensure reproducible results. TA Instrument TRIOS software is used to determine peak temperature and enthalpy of each thermal event. A thermogram of an empty sealed aluminum pan collected using identical instrument parameters as the sample is subtracted from the sample thermogram to remove any instrumentation systematic errors. The thermocouple which measures the heat flow during DSC measurements has an uncertainty of 0.01 °C. For visual comparison, because the heat flow is directly proportional to the heating rate, the reported heat flows from the DSC thermograms are normalized to each heating rate in accordance with eq 1

$$Q_{norm} = Q_{exp} \times \left(\frac{(Q/t)_{ref}}{(Q/t)_{exp}} \right) \quad (1)$$

where Q_{exp} is phase transition heating flow, $(Q/t)_{ref}$ is the reference heating rate of 1 °C min^{-1}, and $(Q/t)_{exp}$ is the experimental heating rate.

Transmission vibrational spectroscopy measurements are performed using a Thermo-Nicolet (Waltham, MA, USA) iS50 Fourier transform spectrometer with a liquid nitrogen-cooled MCT-A detector. Transmission spectra are acquired by signal averaging 10 scans at 4 cm^{-1} resolution with an optical velocity of 1.8988. Each sample is prepared with ∼3 μL (0.5 μL uncertainty from pipet volume due to viscous sample) of IL held between two UV-grade CaF_2 salt plates. The CaF_2 plates are cleaned with acetone and dried under a stream of ultrahigh purity nitrogen between each measurement. For temperature-controlled IR measurements, temperature programs are applied to the transmission IR cell via an International Crystal Laboratories (Garfield, NJ, USA) CryoTherm temperature control apparatus, equipped with multiple thermocouples to monitor temperatures in and around the sample compartment. Before sample spectra are collected, the IL is brought to 120 °C for 30 min to remove residual water from all surfaces. The apparatus is then returned to 30 °C and equilibrated there before an initial spectrum is acquired. To correct for small changes in transmission and reflectivity across the temperature profile, background spectra are taken with the CaF_2 plates from 30 to −75 °C at 10 °C intervals. The sample is cooled to −75 °C at controlled rates, akin to DSC and then heated from −75 to 30 °C at similarly controlled rates with a rate uncertainty of 0.5 °C min^{-1}. IR transmission measurements are replicated at least three times on independent samples to ensure reproducible results.

3. RESULTS

3.1. [N1114] [TFSI] Thermal Analysis. DSC measures heat flows in to or out of a sample which often correlate with morphological or phase changes of the material being examined. Our study uses DSC and temperature-controlled transmission IR spectroscopy data to characterize these transitions and identify which are a function of the heating rate applied. Figure 1 shows the response of [N1114] [TFSI] between 30 and −100 °C. This sample was cooled at 15 °C min^{-1} and heated at 10 °C min^{-1}. The single-phase transition upon cooling is a broad crystallization centered near −45 °C. Upon heating, the thermogram shows several phases and transitions including a glass transition at −75 °C (T_g) exothermic cold crystallization (T_{cc}) at −45 °C, an exothermic solid−solid phase transition (T_{ss}) at −34 °C, a partial melting transition (T_{pm}) at 12 °C, and a complete melting transition (T_{cm}) at 17 °C.

Figure 2 shows the DSC heating traces of [N1114] [TFSI] at rates of 1 °C min^{-1} (black), 5 °C min^{-1} (red), 10 °C min^{-1} (green), and 15 °C min^{-1} (blue). All samples were cooled at

DOI: 10.1021/acs.jpcb.9b01650
J. Phys. Chem. B 2019, 123, 4757−4765

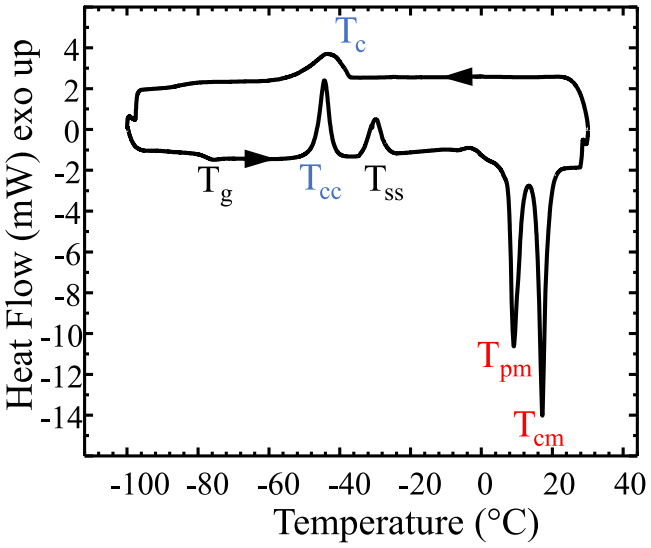

Figure 1. DSC trace of [N1114] [TFSI] between 30 and −100 °C. The sample is cooled at 15 °C min^{-1} and heated at 10 °C min^{-1}. The phase transitions include an glass transition (*T*g), exothermic cold crystallization (*T*cc), an exothermic solid−solid phase transition (*T*ss), a partial melting transition (*T*pm), and a complete melting transition (*T*cm).

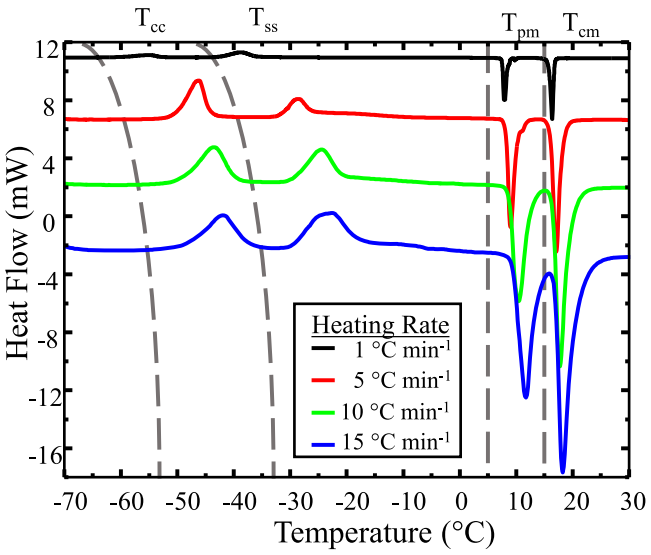

Figure 2. DSC data from heating traces for [N1114] [TFSI] with varied heating rates of 1 °C min^{-1} (black), 5 °C min^{-1} (red), 10 °C min^{-1} (green), and 15 °C min^{-1} (blue). All samples were cooled from 40 to −75 °C at 15 °C min^{-1} prior to heating.

15 °C min^{-1}. Each trace contains a cold crystallization (T_{cc}), solid−solid (T_{ss}), partial melting (T_{pm}), and complete melting (T_{cm}) phase transition. The data in Figure 2 show that the temperature and enthalpy of T_{cc} and T_{ss} vary as a function of the heating rate. The partial melting and complete melting phase transitions are in stable thermodynamic equilibrium because they do not vary with the cooling/heating rate, but the variance in the cold crystallization and solid−solid phase transitions reveals that the possible metastable thermodynamic equilibria resulted from the phase transitions.[21,22]

Figure 3 provides phase transition peak temperatures for [N1114] [TFSI], plotted with respect to the applied heating rate. Each of the four phase transitions are separated into

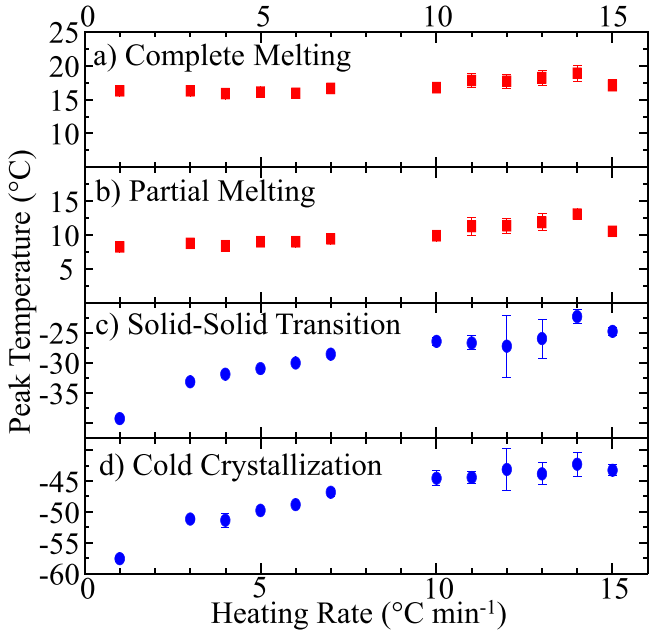

Figure 3. Peak temperature for the four thermal events seen in DSC traces for [N1114] [TFSI], plotted as a function of heating rate. Complete melting (a) and partial melting (b) are plotted in red. The (c) solid−solid transition and (d) cold crystallization are plotted in blue. Error bars are standard pooled deviations from $n > 3$ replicate measurements on $n > 3$ samples.

sections as noted: complete melting (Figure 3a), partial melting (Figure 3b), solid−solid (Figure 3c), and cold crystallization (Figure 3d). The change of peak temperature with respect to the heating rate for the partial melting and complete melting is minimal with a variable range of 8.1−13.6 °C for the partial melting transition and 16.1−19.3 °C for the complete melting transition, respectively. The peak temperatures for each melting phase transition show relatively small decrease with increasing heating rates, which is likely due to thermal lag, but otherwise the melting transitions are stable thermodynamic processes with respect to cooling/heating rate. In direct contrast, the larger change in peak temperature for the cold crystallization and solid−solid transition indicate a significantly larger heating rate effect on these phase transitions.[23,24] The cold crystallization and solid−solid transition exhibit two linear regions, an initial range that rapidly decreases in peak temperature and a second more constant peak temperature range. We define the point each linear range meets the critical heating rate, after which the peak temperature does not change with respect to the heating rate. The peak temperature critical heating rate is 9.1 °C min^{-1} for the cold crystallization and 5.8 °C min^{-1} for the solid−solid transition. The fitted data and fit parameters are detailed in S1.

Figure 4 plots N1114 TFSI phase transition enthalpy as a function of the heating rate. Each phase transition is separated into sections noted as the complete melting (Figure 4a), partial melting (Figure 4b), solid−solid transition (Figure 4c), and cold crystallization (Figure 4d). The complete (Figure 4a) and partial (Figure 4b) melting phase transitions enthalpy change show no trend with respect to heating and are considered thermodynamically stable. The average enthalpy observed for the partial melting is 23.3 ± 1.8 and 26.9 ± 0.7 J g^{-1} for the complete melting phase transition. The small change in enthalpy for both melting phase transitions compared to the

DOI: 10.1021/acs.jpcb.9b01650
J. Phys. Chem. B 2019, 123, 4757−4765

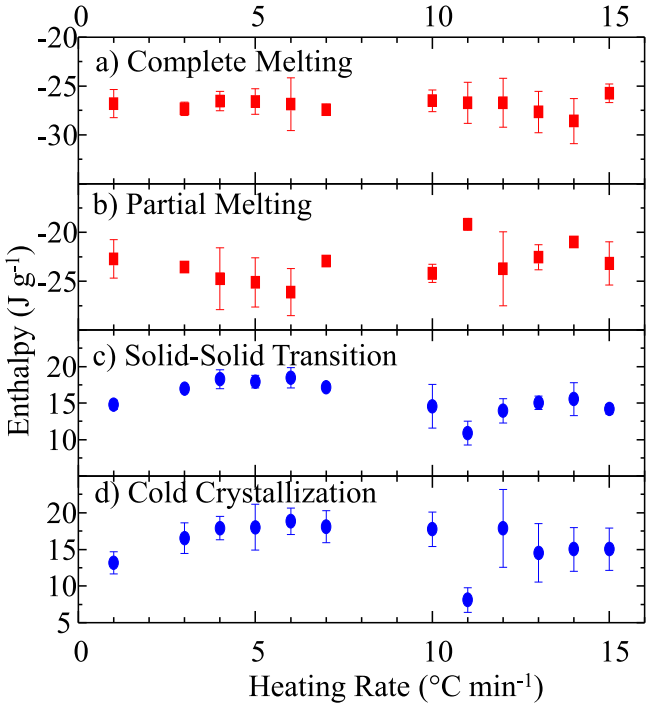

Figure 4. Enthalpy plot of (a) cold crystallization, (b) solid−solid transition, (c) partial melting, and (d) complete melting thermal events seen in the DSC profiles of [N1114] [TFSI] as a function of varied heating rates. All samples are cooled from 40 to −75 °C at 15 °C min^{-1} and then heated from −75 to 40 °C at specified rates. Error bars are standard pooled deviations from $n > 3$ replicate measurements on $n > 3$ samples.

larger change in enthalpy from the cold crystallization and solid−solid phase transitions alludes to the stability of both melting phase transitions. A significant change in enthalpy is observed for the cold crystallization and solid−solid phase transition peaks as a function of heating rates. Data for the solid−solid phase transition from slowest though the fastest heating rates, shown in Figure 4c, show a local maximum of 18.5 J g^{-1} at a 6 °C min^{-1} heating rate. Figure 4d shows a 20% change in enthalpy for the cold crystallization peak (T_{cc}) versus heating rate. A maximum of 18.8 ± 1.4 J g^{-1} is recorded at a 6 °C min^{-1} heating rate, and the enthalpy decreases to minimum values of ca 15 J g^{-1} for the slowest and fastest warming rates probed. The heating rate 11 °C min^{-1} data point for each phase transition does not appear to follow the plot trend, but after preforming over fifteen trials followed by statistical analyses for outliers, the values for the 11 °C min^{-1} heating rate data have been proven to be statistically significant. The maximum enthalpy value indicates that the T_{cc} is most favored at a 5 °C min^{-1} heating rate. The presence of two exothermic transitions upon heating indicates an incomplete phase transition upon fast heating rates, which leads to nonuniform crystalline states within the sample. The nonuniformity within [N1114] [TFSI] correlates with nanodomains, which have previously been reported for [TFSI] anion ILs.[25]

3.2. [N1114] [TFSI] Temperature-Dependent Vibrational Spectroscopy Measurements. Vibrational absorption profiles for each phase are acquired using a variable temperature Fourier transform infrared (VT-FTIR) sampling cell. The maximum heating and cooling rates accessible with the VT-FTIR are 10 °C min^{-1}. VT-FTIR data are shown for [N1114] [TFSI] as it is warmed after being cooled at 5 °C min^{-1} (Figure 5a) and as it is warmed after being cooled at 10 °C min^{-1} (Figure 5b).

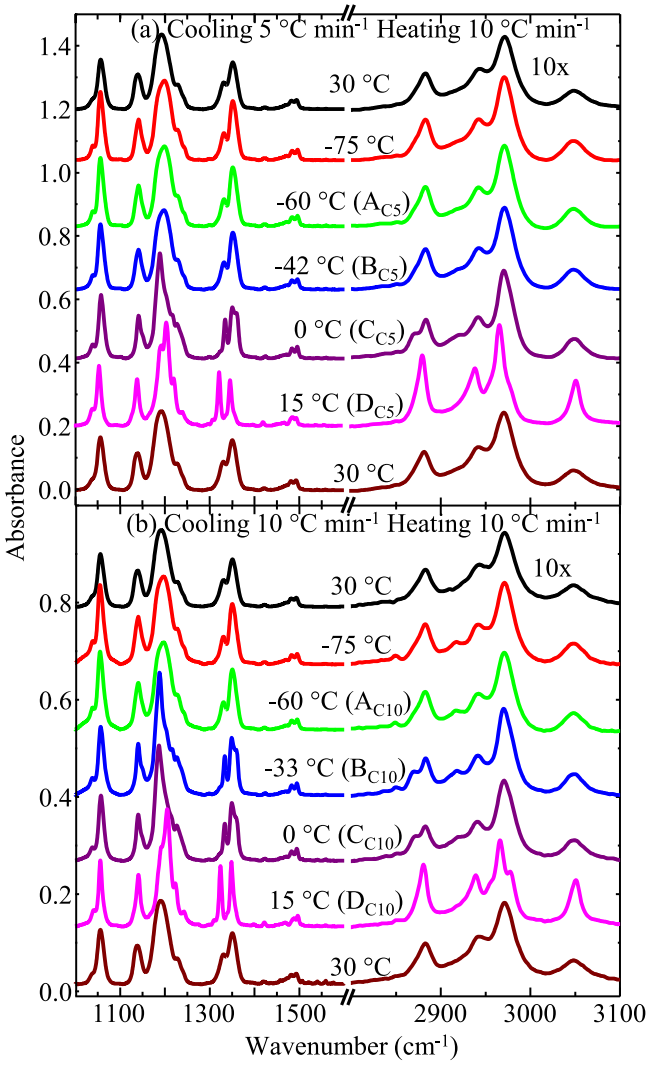

Figure 5. Transmission spectra of [N1114] [TFSI] at varied temperatures. Labels A_{C5} to D_{C5} and A_{C10} to D_{C10} relate to phases as identified in DSC scans. The C−H stretching region of each spectrum (2800−3100 cm^{-1}) has been multiplied by 10× to more clearly show spectral changes.

Temperature-controlled transmission vibrational spectroscopy measurements provide structural and chemical information for each phase transition of [N1114] [TFSI]. Figure 6 shows DSC heating scans of [N1114] [TFSI] when cooled at rates of 5 °C min^{-1} (black) and 10 °C min^{-1} (red) and then heated at a rate of 10 °C min^{-1}. The 5 °C min^{-1} cooling rate exhibits the cold crystallization (T_{cc}), endothermic partial melting (T_{pm}) transition, and endothermic complete melting (T_{cm}) transition, but does not show an exothermic solid−solid (T_{ss}) transition. The 10 °C min^{-1} cooling rate shows the cold crystallization phase transition that is also seen in the 15 °C min^{-1} cooling rate (Figure 2) along with the other transition peaks seen in both cases. Vertical lines labeled A_{C5}, B_{C5}, C_{C5}, and D_{C5} for the 5 °C min^{-1} cooling rate thermogram and A_{C10}, B_{C10}, C_{C10}, and D_{C10} for the 10 °C min^{-1} cooling rate on Figure 6 isolate these phase transitions and identify FTIR acquisition temperature points. Transmission FTIR data acquired at room temperature

DOI: 10.1021/acs.jpcb.9b01650
J. Phys. Chem. B 2019, 123, 4757−4765

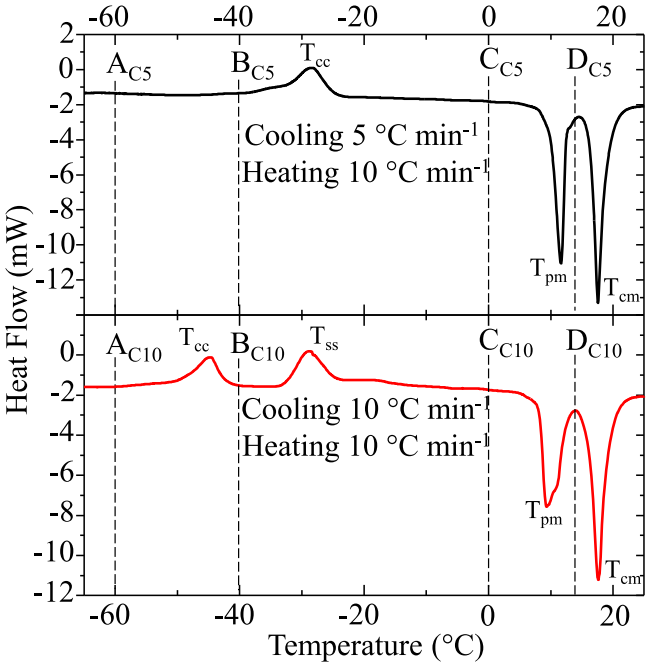

Figure 6. DSC heating scans for [N1114] [TFSI] under different temperature programs. Cooling rate of 5 °C min^{-1} is shown in black (top) cooling rate of 10 °C min^{-1} in shown in red (bottom). Both traces have heating rates of 10 °C min^{-1}. Vertical lines A_{C5}–D_{C5} and A_{C10}–D_{C10} correspond to the temperature-controlled vibrational spectra in figure.

and shown in S2 assign stretching (ν) and bending (δ) vibrational modes for the N1114 cation (red) and TFSI anion (blue).[26,27]

Figure 5 shows FTIR transmission data of [N1114] [TFSI] at varied temperatures that correspond with DSC thermograms in Figure 6. Figure 5a includes spectra collected when the IL was cooled at 5 °C min^{-1} and heated at 10 °C min^{-1} and are listed in order from top to bottom as initial 30 °C (black), −75 °C (red), −60 °C (green, A_{C5}), −42 °C (blue, B_{C5}), 0 °C (purple, C_{C5}), 15 °C (pink, D_{C5}), and final 30 °C (brown). Figure 5b includes spectra collected at 10 °C min^{-1} and heated at 10 °C min^{-1} and are listed in order from top to bottom as initial 30 °C (black), −75 °C (red), −60 °C (green, A_{C10}), −42 °C (blue, B_{C10}), 0 °C (purple, C_{C10}), 15 °C (pink, D_{C10}), and final 30 °C (brown). The temperature points B_{C5} and B_{C10} were taken at different temperatures but represent the same temperature point to ensure that the spectra was taken at a temperature and no phase transition was occurring as seen in Figure 6. When cooled at 5 °C min^{-1}, no change between A_{C5} (green) and B_{C5} (blue) is observed. This is expected from the lack of phase transition in the thermogram acquired under the same conditions as seen in Figure 6 (top, black trace).

4. DISCUSSION

Reports of heating rate effects on ILs are sparse. A recent report by Quitevis and Simon et al. discusses enthalpy and peak temperature of IL phase transitions by observing the cooling rate dependence on the glass transitions of imidazolium-based ILs.[14] The data showed that upon heating, the glass-transition peak temperature and enthalpy decreased with respect to increasing cooling rates.[14] The larger enthalpy associated with phase transitions when the samples are cooled slower corresponds to that a larger amount of energy is needed to regain the ILs molecular mobility from the glass transition upon heating.[14] Slow cooling of the IL creates a higher density glass. Elevating the material from the higher density glassy states and increasing the molecular mobility requires more heat energy which corresponds to increased temperature and endothermic heat transfer.[14] Though previous imidazolium-based ILs research is cooling rate dependent and examines a glass-transition heating process, the molecular mobility principles help explain a general enthalpy trend seen for IL systems' thermodynamic metastable phase transitions. Upon cooling, when crystal nucleation is slow and crystal growth is inhibited, glasses form from the amorphous system.[28] Namely, phase transitions have characteristic amounts of enthalpy needed to regain molecular mobility, and these values change based on heat flux to and from the sample. A metastable thermodynamic state is composed of small displacement of particles that results in a higher energy compared to another state of the same composition and produced in the same conditions, but is held in the metastable state by a constraint to the system.[21,22] These intermediate metastable states can lead to free-energy barriers until the transformation from the metastable into the stable state.[21] It's possible that phase transitions resulting in metastable states can be identified through this analysis. Figures 1 through 5 provide DSC and IR data for IL [N1114] [TFSI] phase transitions. The cold crystallization, solid−solid transition, partial melting, and complete melting phase transitions show differences in change of enthalpy, peak temperature, and vibrational profile. These differences are discussed below to better characterize the effect of the heating rate on [N1114] [TFSI] and broader implications for IL thermochemistry.

4.1. Enthalpy and Peak Temperature of Phase Transitions. The peak temperature for each phase transition shown in Figure 3 decreases with increasing heating rates by a few degrees Celsius. These complete melting (Figure 3a) and partial melting (Figure 3b) features show relatively small increases in the peak temperatures (<5 °C) across the entire range of heating rates examined. This may partially be ascribed to thermal lag, as observed previously at fast heating or cooling rates, and therefore the negligible change due to temperature change rate reveals the melting phase transitions to be in stable thermodynamic equilibria.[23,24] However, the variations are not uniform for the multiple phase transitions observed here. Specifically, the peak temperatures for solid−solid (Figure 3c) and cold crystallization (Figure 3d) phase transitions decrease until reaching an inflection point, at a "critical rate", beyond which the peak temperature no longer changes. Both features show a ca 15 °C range, alluding to the increased amount of energy needed to mobilize the ions, revealing the cold crystallization and solid−solid phase transitions to be in metastable thermodynamic equilibria.

Further, a significant change in enthalpy is observed for the cold crystallization and solid−solid phase transition peaks as a function of heating rates. Specifically, Figure 4d shows a 20% change in enthalpy for the cold crystallization peak (T_{cc}) versus heating rate. A maximum of 18.8 ± 1.4 J g^{-1} is recorded at a 6 °C min^{-1} heating rate, and the enthalpy decreases to minimum values of ca 15 J g^{-1} for the slowest and fastest warming rates probed. The maximum enthalpy value indicates that the T_{cc} transition is maximized at a 6 °C min^{-1} heating rate. The change in enthalpy for the solid−solid phase transition is similar to the enthalpy change for the cold crystallization. This means that these phase transitions may have similarities that

DOI: 10.1021/acs.jpcb.9b01650
J. Phys. Chem. B 2019, 123, 4757−4765

can be identified by characterizing change in enthalpy with respect to heating rates.

Multiple exothermic transitions in a heating trace, such as those shown in Figure 6 indicate the presence of multiple crystalline states within a sample, classified as nanodomains. ILs have previously been correlated with nanodomains, which are specially heterogeneous domains within the IL.[25] Nanodomains have been attributed to the electrostatic interactions between head groups and anion in ILs and are critical to understanding the structure within an IL.[25,29] Ribeiro et al. used Raman data to analyze the multiple exothermic transitions in [N1114] [TFSI] observed with 1 and 5 °C min^{-1} cooling rates.[13] When slowly cooled, the [TFSI] anion is determined to be in the cis conformer and when quickly cooled the [TFSI] anion is in the trans conformer. Our data agree with the prior work and imply that the sample is dominated by trans conformation of the [TFSI] anion after the cold crystallization, with nanodomains of cis conformation due to the fast cooling. The [TFSI] cis conformation has approximately 3.5 kJ mol^{-1} higher energy than the trans conformation; therefore, the presence of the solid−solid transition demonstrates that portions of the sample remains "trapped" in a cis conformer post cold crystallization.[13,30] Specifically, our results show an initial increase in solid−solid phase transition enthalpy until an enthalpy maximum of 18.9 ± 1.8 J g^{-1} at 6 °C min^{-1}, followed by steadily decreasing enthalpy with increasing heating rates (Figure 4b), which indicates an increasing amount of sample "trapped" in cis conformation until the critical heating rate is reached, from which a decreasing amount of the cis [TFSI] conformer persists in the sample. Previous studies suggest that the changing anion in an IL has a larger effect on an IL's thermal stability compared to the cation, and Cao and Mu. suggest that choice of particular anions can introduce significant thermal instability to an IL system.[31] Our data suggest that even driving an IL to a single isomeric form of a given anion, for example, [TFSI], aids in creating uniform thermochemical behavior and strengthens the utility of the IL.

The peak temperature and enthalpy values recorded for complete melting (Figures 3a and 4a) and partial melting (Figures 3 and 4b) phase transitions show insignificant changes with respect to heating rates examined here, especially when compared to the relatively large changes seen for cold crystallization and solid−solid phase transitions. The small change in enthalpy for both melting phase transitions compared to the larger change in enthalpy from the cold crystallization and solid−solid phase transitions supports the stability of both melting phase transitions in terms of the introduced temperature rate bias.

4.2. Phase Transition Vibrational Profiles. When cooling [N1114] [TFSI] from 30 to −75 °C, no significant changes in vibrational profile are observed. Upon reaching −75 °C, the IL is in a "supercooled" state, beyond the freezing point but still in an isotropic (bulk) phase, which is supported by both the lack of thermogram features in the cooling trace and no changes to vibrational mode profiles during cooling (Figures 1 and 5, respectively). Many ILs are known to supercool, and this is generally ascribed to class three ILs reaching a supercooled state that is indicative of the ion mobility,[16] in which DSC heating rate analysis of [N1114] [TFSI] displayed with the large changes in enthalpy and peak temperature of the cold crystallization and solid−solid transition.

Upon warming from −75 °C, [N1114] [TFSI] experiences a glass transition between −75 °C and temperature point A_{C5}/A_{C10} (Figure 1). Glass transitions are described as the sample transition from a glassy amorphous phase to a flexible rubberlike phase.[32] Slight vibrational mode changes associated with this transition are identical for samples cooled at 5 °C min^{-1}(Figure 5a) and 10 °C min^{-1}(Figure 5b) rates. In the $\nu(CF_3)$ region, the large absorbance peak at 1191 cm^{-1} shifts to 1198 cm^{-1}, indicating at least partial crystallization of [N1114] [TFSI]. We attribute this to a bulk phase that is not completely isotropic and instead exhibits stronger dipole−dipole interactions between, and hence an attraction between, $\nu(CF_3)$ groups. This is not surprising as C−F bonds are polar and are known to impart significant dipole−dipole interactions within crystalline materials.[33]

The cold crystallization vibrational profile of [N1114] [TFSI] is reported at temperature point C_{C5} when cooled at 5 °C min^{-1}(Figure 5a) and temperature point B_{C10} when cooled at 10 °C min^{-1}(Figure 5b). The vibrational mode changes associated with the cold crystallization include a growth of a shoulder peak in the $\nu_s(SO_2)$ region at 1150 cm^{-1}. A new absorption feature appears in the $\nu(CF_3)$ region at 1188 cm^{-1}, which is accompanied by a shoulder growth at 1203 cm^{-1} and absorption intensity increase at 1216 cm^{-1}. There is a peak shift in the $\nu_{as}(SO_2)_{op}$ region spanning from 1330 to 1334 cm^{-1}. Finally, a second new absorption appears at 1358 cm^{-1}, assigned to $\nu_{as}(SO_2)_{ip}$ in the high-frequency (CH stretch) region, the peak at 2870 cm^{-1} assigned to $\nu_s(CH_2)$ sharpens to resolve a peak and distinct, low-energy shoulder. The changes in the vibrational profile listed are attributed to increased crystalline character within the IL material. The distinct peaks in the $\nu_s(CH_2)$ region can be further assigned to $\nu_s(N-CH_2)$ at 2870 cm^{-1} and $\nu_s(CH_2-CH_2)$ at 2882 cm^{-1}, with the more intense peak corresponding to the presence of two CH_2 groups. The lower energy, single CH_2 group, is assigned to be attached to the nitrogen center, because of the nitrogen-withdrawing electron density and slightly lowers vibrational frequency. Based on the sharp, well-resolved peaks and the temperature at which they were acquired, we assign these spectral data to correspond to a crystallized IL phase, created from an initially glassy, primarily isotropic molecular environment.[20] Also, the lower frequency region resembles the peak profile of "an ordered thin film" as observed using RAIRS by Hüfft et al.,[20] which further supports the assignment of these data to an increasingly ordered or crystalline state.

Vibrational spectra between temperature points B_{C5}/B_{C10} and C_{C5}/C_{C10} highlight molecular environment changes for the solid−solid transition as compared to the cold crystallization. The vibrational modes at temperature point C_{C5} when cooled at 5 °C min^{-1} mirror the cold crystallization spectra at temperature point B_{C5} seen when cooled at 10 °C min^{-1}, supporting our assignment of both at T_{cc} shown in Figure 6. These changes in the absorbance spectra provide evidence that the cold crystallization peak seen at 28.5 °C in the 5 °C min^{-1} cooling rate DSC scan is the same thermal event seen in the first peak (−44.8 °C) of the 10 °C min^{-1} cooling rate. The presence of the cold crystallization but not the solid−solid phase transition eludes to the cold crystallization being thermodynamically favored. This could be explained by considering that the slower cooling rate allows the IL to crystallize to the favored structure. The solid−solid phase transition might also be present in the thermogram, but the

DOI: 10.1021/acs.jpcb.9b01650
J. Phys. Chem. B 2019, 123, 4757−4765

enthalpy of the cold crystallization is greater, leading to a cold crystallized IL state rather than the phase after the solid−solid-phase transition.

The vibrational spectrum measured at temperature point C_{C10}, showing the solid−solid transition for [N1114] [TFSI] cooled at 10 °C min^{-1}, shows most significant differences in the $\nu(CF_3)$ region when compared to the spectra B_{C10}. There is no longer a shoulder peak at 1202 cm^{-1}, but the absorbance peak at 1216 cm^{-1} develops into a shoulder on the $\nu(CF_3)$ peak. In the high-frequency region for the 10 °C min^{-1} cooling rate (Figure 5b), the peak at 2917 cm^{-1} also becomes a shoulder peak over this temperature range. The changes, though small, correspond to a second phase transformation in the 10 °C min^{-1} cooling. From the vibrational spectra, we assigned the second phase transition to involve primarily the $\nu(CF_3)$ and $\nu(N-CH_3)$ modes, though it is difficult to determine quantitatively because many different modes overlap within this spectral window (1160 to 1250 cm^{-1}). The IR spectroscopy collected here is unable to resolve the [TFSI] anion conformation, but it does support a significant change in the chemical environment of [TFSI].

The partial melting vibrational profile was measured at temperature points D_{C5} and D_{C10}, which is after the partial melting but before the complete melting endothermic features for both traces shown in Figure 6. Similar spectral changes are observed for both the 5 °C min^{-1}(Figure 5a) and 10 °C min^{-1}(Figure 5b) cooling rates. The vibrational mode changes seen for the low frequency include the $\nu(CF_3)$ region with peaks at 1192, 1205, 1223, and 1242 cm^{-1}. Comparison of modes acquired at temperature point D_{C5}/D_{C10} versus the data acquired at 30 °C reveals that these four absorbance bands are smoothed into a single broad peak at 30 °C. Given that the sample at temperature point D_{C5}/D_{C10} is yet to undergo the complete melting phase transition (at 17 °C in Figure 6), and the relatively sharp IR absorbance bands reported here, we propose that the sample exists in a partially ordered form between the partial melting and complete melting thermal features. The persistence of well-defined peaks is surprising to and again relates to the presence of frozen domains remaining in the sample even at this relatively warm temperature. Because the sharp vibrational modes are replicated in both cooling rates, the frozen domains may dominate the IL at this temperature to the point, but the enthalpy of each melting transition, seen in Figure 4, are nearly equal. Therefore, the frozen domains may remain clustered, lending to the sharp vibrational modes seen in the spectra. Additional significant changes are seen in the $\nu_{as}(SO_2)_{op}$ and $\nu_{as}(SO_2)_{ip}$ regions. The $\nu_{as}(SO_2)_{op}$ peak shifts from 1333 to 1324 cm^{-1}. The $\nu_{as}(SO_2)_{ip}$ region also develops a new absorbance feature at 1339 cm^{-1}, while still maintaining the 1348 cm^{-1} peak. By contrast the high-frequency region shows only subtle changes, including a significantly sharper peak at 2966 cm^{-1} upon warming in both cooling rates. The sample cooled at 10 °C min^{-1} maintains a shoulder peak at 2917 cm^{-1} and has a new absorption feature at 2977 cm^{-1}. The 5 °C min^{-1} cooling rate contains an additional small shoulder peak at ca 2975 cm^{-1} that is poorly resolved. Combining interpretation of DSC thermogram data and the spectral changes at temperature point D_{C5}/D_{C10} suggests an incomplete melting transition, which results in a mixture of ordered and amorphous states.

The IL interactions after the complete melting phase transition are shown by IR data acquired at 30 °C for both the 5 and 10 °C min^{-1} cooling rates. Here the vibrational profile reproduces the original room temperature (30 °C) data set exactly. The 30 °C point is after the complete melting phase transition that is seen in the DSC scan, so and our IR data and DSC data indicate that the sample is returned to the isotropic bulk liquid phase.

Judicious control of heating and cooling rates may provide a pathway to favorably manipulate an IL's phase transitions. After cooling [N1114] [TFSI] at 15 °C min^{-1}, the heating rate manipulation showed distinct changes in enthalpy and peak temperature between phase transitions, but the critical information lies within understanding how these changes affect the molecular environment and molecular mobility for the multiple phases. Previous studies show that ammonium-based cations with the [TFSI] anion increase in glass-transition temperature when carbon chain length increased, which indicated a decrease in degrees of rotational freedom.[34,35] There is currently sparse experimental data available for [N1114] paired with anions other than [TFSI]. This study and further spectroscopic research into anion effects on ammonium-based IL will strengthen the molecular understanding of this complex class of ILs.

A second useful outcome of this work is significant evidence that melting phase transitions might be classified by their constant energy flow with respect to changing heating and cooling rates.[36] Both melting transitions observed here have negligible changes in enthalpy or peak temperature versus heating rates. In contrast, there are significant changes in enthalpy and peak temperatures versus heating rates for the cold crystallization and solid−solid phase transitions. Using these metrics to assign stable and metastable thermochemistry features in ILs is novel, but a similar approach has been utilized to assign phase changes in polymers.[37] Both classes of materials have complex intermolecular interactions and often exhibit slow phase transition dynamics. Thermochemistry data for amorphous poly(trimethylene terephthalate) (PTT) show a clear correlation between the amount of strain on the PTT film and molecular organization. The DSC analysis of PTT shows that the increase in global molecular order leads to a decrease in cold crystallization temperature, until the molecular order reaches a critical value where the cold crystallization no longer takes place.[37] This conclusion that the magnitude of polymer order affects the cold crystallization coincides with the effect of the heating rate on cold crystallization seen in [N1114] [TFSI]. When the IL is cooled at 15 °C min^{-1}, it reaches a supercooled state where is has not yet crystallized, as seen in the VT-FTIR data, which leaves a relatively large fraction of the liquid able to reorganize in a cold crystallization transition.[13] Furthermore, the total enthalpy of cold crystallization versus heating rate reaches a local maximum before decreasing, expanding on the polymer conclusion that increased disorder leads to increased cold crystallization; there seems to be a system-dependent limit of cold crystallization. After the cold crystallization enthalpy critical point with increasing heating rates, therefore increased disorder, domains within the sample are not able to cold crystallize. Therefore, sample tunability becomes possible just by altering the heating rate and inhibiting domain crystallization.

5. CONCLUSION

The combination of DSC data with temperature-controlled IR measurements show that [N1114] [TFSI] phase transitions exhibit clear dependence on heating and cooling rates. The

DOI: 10.1021/acs.jpcb.9b01650
J. Phys. Chem. B 2019, 123, 4757−4765

enthalpy for the phase transitions and peak temperatures at which the phase transitions take place reveal characteristic features indicative of a cold crystallization, solid−solid, and melting phase transitions. Transmission FTIR spectra acquired for samples exposed to different heating and cooling rates provide structural details of the associated transitions and phases and show clear dependence on the temperature programs applied, which correspond to changes in the DSC thermograms. Upon warming, we observe significant changes in multiple vibrational modes, which suggest that multiple crystallization polymorphs are accessible, again depending on the temperature ramp rates. Specifically, two distinct vibrational profiles are associated with the 10 °C min^{-1} cooling rate, indicating a distinct crystallization and melting pathway when compared to slower cooling rates. All cooling and heating rates result in identical initial and final spectrum at 30 °C, eliminating the possibility of thermal degradation or other irreversible chemical changes.

These results provide important suggestions of crystalline forms of [N1114] [TFSI] and of IL phase transitions as they pertain to the class assignments. Clearly, there are IL phases which may only be accessed by specific growth conditions or temperature programs. Significant evidence indicates that these various phases and phase transitions are driven by preferred orientations of the [TFSI] anion, as each crystallization transmission vibrational spectrum showed distinct changes in the SO_2 and CF_3 regions. Existing and future studies of IL phase transitions will be important to determine what phases the materials adopt under varying environmental conditions, how these phases affect physicochemical properties, and what general trends may be available to predict the performance of tailored materials.[38−42]

■ ASSOCIATED CONTENT

Supporting Information

The Supporting Information is available free of charge on the ACS Publications website at DOI: 10.1021/acs.jpcb.9b01650.

Peak temperature versus heating rate plots for the cold crystallization and solid−solid transition with raw data and exponential fits; room temperature bulk FTIR spectrum of [N1114] [TFSI] with vibrational modes assignments and a structure of [N1114] [TFSI] with numbered atoms is provided to correlate to the vibrational mode assignments.; and table of wavenumbers associated with each assigned vibrational mode associated with [N1114] [TFSI] (PDF)

■ AUTHOR INFORMATION

Corresponding Author

*E-mail: jaclyn-wrona@uiowa.edu.

ORCID

Jaclyn N. Curry: 0000-0003-2007-9484

Scott K. Shaw: 0000-0003-3767-3236

Notes

The authors declare no competing financial interest.

■ ACKNOWLEDGMENTS

The authors gratefully acknowledge funding support from the National Science Foundation (CHE-1651381) and the Research Corporation in the form of a Cottrell Scholar Award. JC expresses her gratitude to the University of Iowa Graduate College for fellowship support during a portion of this work. We also gratefully acknowledge the support of dedicated staff members in the glass shop, electronics shop, and machine shops (physics and engineering) at the University of Iowa, which greatly supported the development of equipment and materials used in this work.

■ REFERENCES

(1) Anaredy, R. S.; Shaw, S. K. Long-Range Ordering of Ionic Liquid Fluid Films. *Langmuir* **2016**, *32*, 5147−5154.

(2) Atkin, R.; Warr, G. G. Structure in Confined Room-Temperature Ionic Liquids. *J. Phys. Chem. C* **2007**, *111*, 5162−5168.

(3) Hough, W. L.; Rogers, R. D. Ionic Liquids Then and Now: From Solvents to Materials to Active Pharmaceutical Ingredients. *Bull. Chem. Soc. Jpn.* **2007**, *80*, 2262−2269.

(4) Johnson, K. What's an Ionic Liquid. *Electrochem. Soc. Interface* **2007**, *16*, 38−41.

(5) Kelley, S. P.; Narita, A.; Holbrey, J. D.; Green, K. D.; Rogers, R. D. Understanding the Effects of Ionicity in Salts, Solvates, Co-Crystals, Ionic Co-Crystals, and Ionic Liquids, Rather than Nomenclature, Is Critical to Understanding Their Behavior. *Cryst. Growth Des.* **2013**, *13*, 965−975.

(6) Paschoal, V. H.; Faria, L. F. O.; Ribeiro, M. C. C. Vibrational Spectroscopy of Ionic Liquids. *Chem. Rev.* **2017**, *117*, 7053−7112.

(7) Adawiyah, N.; Moniruzzaman, M.; Hawatulaila, S.; Goto, M. Ionic Liquids as a Potential Tool for Drug Delivery Systems. *MedChemComm* **2016**, *7*, 1881−1897.

(8) Aliaga, C.; Santos, C. S.; Baldelli, S. Surface Chemistry of Room-Temperature Ionic Liquids. *Phys. Chem. Chem. Phys.* **2007**, *9*, 3683−3700.

(9) Aslanov, L. A. Ionic Liquids: Liquid Structure. *J. Mol. Liq.* **2011**, *162*, 101−104.

(10) McFarlane, J.; Ridenour, W. B.; Luo, H.; Hunt, R. D.; DePaoli, D. W.; Ren, R. X. Room Temperature Ionic Liquids for Separating Organics from Produced Water. *Sep. Sci. Technol.* **2005**, *40*, 1245−1265.

(11) Somers, A.; Howlett, P.; MacFarlane, D.; Forsyth, M. A Review of Ionic Liquid Lubricants. *Lubricants* **2013**, *1*, 3−21.

(12) Sun, S.; Duan, Z.; Wang, X.; Lai, G.; Zhang, X.; Wei, H.; Liu, L.; Ma, N. Cheap, Flexible, and Thermal-Sensitive Paper Sensor through Writing with Ionic Liquids Containing Pencil Leads. *ACS Appl. Mater. Interfaces* **2017**, *9*, 29140−29146.

(13) Faria, L. F. O.; Matos, J. R.; Ribeiro, M. C. C. Thermal Analysis and Raman Spectra of Different Phases of the Ionic Liquid Butyltrimethylammonium Bis(trifluoromethylsulfonyl)imide. *J. Phys. Chem. B* **2012**, *116*, 9238−9245.

(14) Tao, R.; Gurung, E.; Cetin, M. M.; Mayer, M. F.; Quitevis, E. L.; Simon, S. L. Fragility of Ionic Liquids Measured by Flash Differential Scanning Calorimetry. *Thermochim. Acta* **2017**, *654*, 121−129.

(15) Shimizu, Y.; Fujii, K.; Imanari, M.; Nishikawa, K. Phase Behavior of a Piperidinium-Based Room-Temperature Ionic Liquid Exhibiting Scanning Rate Dependence. *J. Phys. Chem. B* **2015**, *119*, 12552−12560.

(16) Fredlake, C. P.; Crosthwaite, J. M.; Hert, D. G.; Aki, S. N. V. K.; Brennecke, J. F. Thermophysical Properties of Imidazolium-Based Ionic Liquids. *J. Chem. Eng. Data* **2004**, *49*, 954−964.

(17) Robinson, J. W.; Frame, E. M. S.; Frame, G. M., *Undergraduate Instrumental Analysis*, 6th ed.; Marcel Dekker: New Youk, 2005.

(18) Hunger, J.; Roy, S.; Grechko, M.; Bonn, M. Dynamics of Dicyanamide in Ionic Liquids is Dominated by Local Interactions. *J. Phys. Chem. B* **2019**, *123*, 1831.

(19) Holbrey, J. D.; Seddon, K. R. The Phase Behaviour of 1-Alkyl-3-methylimidazolium Tetrafluoroborates; Ionic Liquids and Ionic Liquid Crystals. *J. Chem. Soc., Dalton Trans.* **1999**, 2133−2140.

(20) Höfft, O.; Bahr, S.; Kempter, V. Investigations with Infrared Spectroscopy on Films of the Ionic Liquid [EMIM]Tf2N. *Langmuir* **2008**, *24*, 11562−11566.

DOI: 10.1021/acs.jpcb.9b01650
J. Phys. Chem. B 2019, 123, 4757−4765

(21) Kauzmann, W. The Nature of the Glassy State and the Behavior of Liquids at Low Temperatures. *Chem. Rev.* **1948**, *43*, 219−256.
(22) Anderson, G., *Stable and Metastable Equilibrium: The Third Constraint*; The Geochemical Society Special Publication; Elsevier, 2002; Vol. 7.
(23) Whiting, L. F.; Carr, P. W. Effect of Thermal Lag and Measurement Precision in Differential Scanning Calorimetry: Theoretical Guidelines for Enzyme-Substrate Reactions by the Method of Orthogonal Collocation. *Anal. Chem.* **1978**, *50*, 1997−2006.
(24) Leharne, S. The Physical Chemistry of High-Sensitivity Differential Scanning Calorimetry of Biopolymers. *ChemTexts* **2016**, *3*, 1−12.
(25) Wang, Y.; Voth, G. A. Tail Aggregation and Domain Diffusion in Ionic Liquids. *J. Phys. Chem. B* **2006**, *110*, 18601−18608.
(26) Hanke, K.; Kaufmann, M.; Schwaab, G.; Havenith, M.; Wolke, C. T.; Gorlova, O.; Johnson, M. A.; Kar, B. P.; Sander, W.; Sanchez-Garcia, E. Understanding the Ionic Liquid [NC4111][NTf2] from Individual Building Blocks: A IR-spectroscopic Study. *Phys. Chem. Chem. Phys.* **2015**, *17*, 8518−8529.
(27) Socrates, G., *Infrared and Raman Characteristic Group Frequencies: Tables and Charts*, 3rd ed.; John Wiley & Sons Inc.: Hoboken, NJ, 2001.
(28) Angell, C. A.; Richards, B. E.; Velikov, V. Simple Glass-Forming Liquids: Their Definition, Fragilities, and Landscape Excitation Profiles. *J. Phys.: Condens. Matter* **1999**, *11*, A75.
(29) Araque, J. C.; Hettige, J. J.; Margulis, C. J. Modern Room Temperature Ionic Liquids, a Simple Guide to Understanding Their Structure and How It May Relate to Dynamics. *J. Phys. Chem. B* **2015**, *119*, 12727−12740.
(30) Lima, T. A.; Paschoal, V. H.; Faria, L. F. O.; Ribeiro, M. C. C.; Ferreira, F. F.; Costa, F. N.; Giles, C. Comparing Two Tetraalkylammonium Ionic Liquids. II. Phase Transitions. *J. Chem. Phys.* **2016**, *144*, 224505.
(31) Cao, Y.; Mu, T. Comprehensive Investigation on the Thermal Stability of 66 Ionic Liquids by Thermogravimetric Analysis. *Ind. Eng. Chem. Res.* **2014**, *53*, 8651−8664.
(32) Skoog, D.; Holler, F. J.; Crouch, S., *Principles of Instrumental Anaysis*, 6th ed.; Thomson Corporation: Belmont, CA, 2007.
(33) Murray-Rust, P.; Stallings, W. C.; Monti, C. T.; Preston, R. K.; Glusker, J. P. Intermolecular Interactions of the Carbon-Fluorine Bond: The Crystallographic Environment of Fluorinated Carboxylic Acids and Related Structures. *J. Am. Chem. Soc.* **1983**, *105*, 3206−3214.
(34) Sun, J.; Forsyth, M.; MacFarlane, D. R. Room-Temperature Molten Salts Based on the Quaternary Ammonium Ion. *J. Phys. Chem. B* **1998**, *102*, 8858−8864.
(35) Xu, W.; Cooper, E. I.; Angell, C. A. Ionic Liquids: Ion Mobilities, Glass Temperatures, and Fragilities. *J. Phys. Chem. B* **2003**, *107*, 6170−6178.
(36) Atkins, P. W., *Atkins' Physical Chemistry*, 8th ed. ed.; Oxford University Press: Oxford New York, 2006.
(37) Vasanthan, N.; Manne, N. J.; Krishnama, A. Effect of Molecular Orientation on the Cold Crystallization of Amorphous−Crystallizable Polymers: The Case of Poly(trimethylene terephthalate). *Ind. Eng. Chem. Res.* **2013**, *52*, 17920−17926.
(38) Zheng, W.; Mohammed, A.; Hines, L. G.; Xiao, D.; Martinez, O. J.; Bartsch, R. A.; Simon, S. L.; Russina, O.; Triolo, A.; Quitevis, E. L. Effect of Cation Symmetry on the Morphology and Physicochemical Properties of Imidazolium Ionic Liquids. *J. Phys. Chem. B* **2011**, *115*, 6572−6584.
(39) Hettige, J. J.; Araque, J. C.; Margulis, C. J. Bicontinuity and Multiple Length Scale Ordering in Triphilic Hydrogen-Bonding Ionic Liquids. *J. Phys. Chem. B* **2014**, *118*, 12706−12716.
(40) Imai, Y.; Abe, H.; Yoshimura, Y. X-ray Diffraction Study of Ionic Liquid Based Mixtures. *J. Phys. Chem. B* **2009**, *113*, 2013−2018.
(41) Mars, J.; Hou, B.; Weiss, H.; Li, H.; Konovalov, O.; Festersen, S.; Murphy, B. M.; Rütt, U.; Bier, M.; Mezger, M. Surface Induced Smectic Order in Ionic Liquids - An X-ray Reflectivity Study of [C22C1im]+[NTf2]. *Phys. Chem. Chem. Phys.* **2017**, *19*, 26651−26661.
(42) Sloutskin, E.; Ocko, B. M.; Tamam, L.; Kuzmenko, I.; Gog, T.; Deutsch, M. Surface Layering in Ionic Liquids: An X-ray Reflectivity Study. *J. Am. Chem. Soc.* **2005**, *127*, 7796−7804.

DOI: 10.1021/acs.jpcb.9b01650
J. Phys. Chem. B 2019, 123, 4757−4765